Dissecting Regional Variations in Stress Fiber Mechanics in Living Cells with Laser Nanosurgery

Kandice Tanner,[†‡] Aaron Boudreau,[†] Mina J. Bissell,[†] and Sanjay Kumar[†‡*]
[†]Lawrence Berkeley National Laboratory and [‡]University of California, Berkeley, California

ABSTRACT The ability of a cell to distribute contractile stresses across the extracellular matrix in a spatially heterogeneous fashion underlies many cellular behaviors, including motility and tissue assembly. Here we investigate the biophysical basis of this phenomenon by using femtosecond laser nanosurgery to measure the viscoelastic recoil and cell-shape contributions of contractile stress fibers (SFs) located in specific compartments of living cells. Upon photodisruption and recoil, myosin light chain kinase-dependent SFs located along the cell periphery display much lower effective elasticities and higher plateau retraction distances than Rho-associated kinase-dependent SFs located in the cell center, with severing of peripheral fibers uniquely triggering a dramatic contraction of the entire cell within minutes of fiber irradiation. Image correlation spectroscopy reveals that when one population of SFs is pharmacologically dissipated, actin density flows toward the other population. Furthermore, dissipation of peripheral fibers reduces the elasticity and increases the plateau retraction distance of central fibers, and severing central fibers under these conditions triggers cellular contraction. Together, these findings show that SFs regulated by different myosin activators exhibit different mechanical properties and cell shape contributions. They also suggest that some fibers can absorb components and assume mechanical roles of other fibers to stabilize cell shape.

INTRODUCTION

It is becoming increasingly appreciated that the mechanical balance between tensile prestress in the cellular cytoskeleton and the elastic resistance of the extracellular matrix (ECM) can strongly regulate a wide variety of fundamental cellular properties, including shape, polarity, motility, and fate decisions. Alterations to this balance have been demonstrated in a number of settings to induce proliferation and apoptosis, malignant transformation, and loss of tissue structural integrity (1–6). In cultured mammalian cells, actomyosin stress fiber bundles (or stress fibers (SFs)) are perhaps the most significant and widely studied generators of contractile forces. These structures, which are composed of antiparallel arrays of F-actin stabilized by actin-binding proteins and interleaved with nonmuscle myosin II (NMMII), contribute to cytoskeletal prestress by anchoring into cell-ECM adhesions and permitting the cell to generate traction against the ECM (7–9). The contractile activity of SFs requires phosphorylation of the regulatory myosin light chain (MLC), which in turn is largely promoted by the activity of two enzymes: Rho-associated kinase (ROCK), which primarily acts by inactivating MLC phosphatase, and myosin light chain kinase (MLCK), which directly phosphorylates MLC. ROCK and MLCK themselves are activated through distinct signaling pathways: ROCK is a direct effector of Rho GTPase, and MLCK is activated through a Ca^{++}/calmodulin-dependent mechanism (10–14).

Although it is widely agreed that both ROCK and MLCK contribute to SF function, the specific and differential contributions of each regulatory enzyme to SF contractile mechanics remain incompletely understood. The seminal work of Katoh et al. (15,16) and Totsukawa et al. (17) led to a model in which ROCK and MLCK preferentially govern SF assembly and contractility according to the location of the SF within the cell. Specifically, SFs can be divided into subpopulations of MLCK-controlled peripheral SFs that follow the exterior contours of the cell and are dissipated after MLCK inhibition, and ROCK-controlled central SFs that span the cellular interior and are lost after ROCK inhibition. Subsequent ultrastructural studies suggested that these two populations of SFs have different architectures, with the F-actin-based bundles in peripheral SFs appearing thicker and longer than their central counterparts (15). These findings prompt the question of whether regional regulation of SF function also produces or reflects mechanical differences between these SF populations, i.e., whether central and peripheral SFs bear distinct contractile properties, and whether they contribute in distinct ways to the shape the stability of the entire cell. In the most direct attempt to address this question to date, Katoh and colleagues (15) found that central and peripheral SFs isolated from cultured cells and treated with Ca^{2+} and Mg-ATP contract at similar rates but with different timing of onset, hinting at, but not showing clearly, differences in contractile mechanics. The interpretation of this result was further complicated by the fact that SF isolation requires chemical and mechanical removal of the rest of the cell, including some components of the cytoskeleton and adhesive machinery. Thus, whether central and peripheral SFs bear distinct mechanical properties has remained a significant open question in the field, and attempts to resolve it have been severely limited by the absence of methods capable

Submitted March 2, 2010, and accepted for publication August 20, 2010.

*Correspondence: skumar@berkeley.edu

Editor: Douglas Nyle Robinson.

0006-3495/10/11/2775/9 $2.00

doi: 10.1016/j.bpj.2010.08.071

of selectively probing the microscale mechanical properties of single SFs in living cells.

We recently showed that irradiation with focused femtosecond laser pulses (femtosecond laser nanosurgery) can be used to photodisrupt single SFs in living cells with submicron spatial resolution and without damaging adjacent SFs or the plasma membrane (18). Upon photodisruption, a single SF retracts with recoil dynamics consistent with a Kelvin-Voigt model of a viscoelastic cable, with inhibition of NMMII activators ROCK or MLCK reducing the rate and extent of SF retraction. We and others (19–21) have since applied this method to investigate the microscale sarcomeric mechanics of SFs, the contribution of SF-induced tension to focal adhesion dynamics (22), and the contributions of actomyosin bundles to cell-cell adhesion within epithelia (23). Thus, femtosecond laser nanosurgery possesses a unique ability to selectively interrogate the mechanics of single SFs at specific locations within living cells and should, in principle, be capable of detecting differences in the mechanics and cell-shape contributions of central and peripheral SFs.

Here, we use femtosecond laser nanosurgery to investigate the differential mechanics and cell-shape contributions of central and peripheral SFs in human glioma cells. We show that pharmacological inhibition of ROCK and MLCK leads to disruption of central and peripheral SFs, respectively, consistent with previous studies in fibroblasts. We then measure the viscoelastic properties and morphological contributions of each SF population. We find that each SF population bears distinct viscoelastic properties, and that severing peripheral fibers induces whole-cell contraction on the timescale of minutes. Moreover, pharmacological dissipation of peripheral SFs causes central SFs to adopt viscoelastic retraction and cell-shape contributions similar to those of peripheral SFs in untreated cells. These results show that SFs in different portions of the cell and under the regulation of different myosin activators possess distinct mechanical properties and cell-shape contributions, and hint at the unique potential of femtosecond laser nanosurgery for spatially mapping the microscale contractile mechanics of living cells.

MATERIALS AND METHODS

Cell culture and sample preparation

Human glioma cell lines U87MG and U373MG were cultured as previously described (5). For imaging, cells were trypsinized (Trypsin-EDTA; Gibco, Grand Island, NY), harvested, and replated on 35 mm, 1.5 coverslip-bottomed petri dishes, (0.16–0.19 mm; Mat Tek, Ashland, MA) that had been precoated with pepsin-solubilized bovine tail collagen (PureCol; Advanced Biomatrix, San Diego, CA). For ROCK and MLCK inhibition, cells were pretreated with 5 μM Y-27632 (Calbiochem, San Diego, CA) or 10 μM ML-7 (Sigma, St. Louis, MO), respectively, for 1 h before imaging. We previously demonstrated that treatment of U373MG cells with either Y-27632 or ML-7 under conditions of 5–10 μM showed a reduction in MLC phosphorylation by Western blot (24).

LifeAct molecular cloning and lentiviral expression

Wild-type mCherry was amplified by polymerase chain reaction from a donor plasmid (pLENTIR4R2V5-DEST UbC-mCherry, kindly provided by Curt Hines, Lawrence Berkeley National Laboratory, Berkeley, CA) to incorporate a unique N-terminal NheI site. Sense and antisense oligonucleotides encoding the first 17 residues of *Saccharomyces cerevisiae* ABP140 (MGVADLIKKFESISKEE) and a flexible linker (GDPPVAT) (25) were subcloned in frame with the mCherry N-terminus to yield LifeAct-mCherry, which was subsequently cloned into pENTR1A (Invitrogen, Carlsbad, CA). Once in pENTR1A, the LifeAct-mCherry was recombined into pLenti-CMV/TO-Puro-DEST#2 (kindly provided by Eric Campeau, Lawrence Berkeley National Laboratory) using LR Clonase II (Invitrogen). For lentiviral production, pLenti-CMV/TO-Puro LifeAct-mCherry was cotransfected with pLP1, pLP2, and pLP-VSVG helper plasmids into 293FT host cells (all from Invitrogen) using Fugene6 transfection reagent (Roche, Indianapolis, IN). Viral supernatants were used to infect cells in the presence of 4 μg/mL polybrene, and cell lines were stably selected with puromycin.

Immunofluorescence

For immunofluorescence, samples were rinsed twice with phosphate-buffered saline (PBS; Fisher Scientific, Pittsburgh, PA), fixed with 4% paraformaldehyde solution for 10 min, permeabilized with 0.5% Triton X-100 for 10 min, and rinsed and blocked in 5% bovine serum albumin for 1 h at room temperature. Cells were then incubated for 1 h at room temperature in mouse anti-MLC IgG (1:200; Sigma) in PBS at the specified dilutions. After incubation with primary antibody, the cells were rinsed twice with PBS and then incubated with Alexa Fluor-543 goat anti-mouse IgG 219 (1:500; Invitrogen), and Alexa Fluor-488-phalloidin (1:200; Invitrogen) for 1 h at room temperature. Cell nuclei were then labeled with DAPI (1:500; Invitrogen). Images were acquired with an upright Zeiss LSM 710 Meta confocal microscope (Jena, Germany). One-photon, confocal, two-dimensional images of 512 $\times$ 512 pixels (lateral dimensions) were acquired with a 1.4 NA 63$\times$ oil-immersion objective using a zoom corresponding to an area of 70 $\times$ 70 μm^2. We simultaneously excited our sample with the 488 nm line from an argon ion laser with a power of $<$3% (total power 30 mW) and 546 nm from a solid-state laser (power of $<$10%). A secondary dichroic mirror, SDM 560, was employed in the emission pathway to separate the red (band-pass filters 560–575 nm) and green (band-pass filters 505–525 nm) channels at a gain of 400 on the amplifier. High-resolution movies were also obtained with a Zeiss LSM 710 Meta confocal microscope, with settings tuned for mCherry excitation/emission (543 nm/596 nm) and with an image acquisition rate of one frame per second. The laser power for the 543 nm setting was set at $<$3% of the maximum power and the gain on the detectors was set to 450.

Laser nanosurgery of SFs

All nanosurgery experiments were performed on a Zeiss LSM 510 Meta confocal microscope equipped with a mode-locked MaiTai Ti:sapphire femtosecond laser (Spectra Physics, Newport Beach, CA) based on previously published protocols (18). First, one-photon fluorescence images were obtained by illuminating samples with 543 nm (HeNe laser, maximum power 1 mW). For nanosurgery we employed a 1.4-NA 63$\times$ oil-immersion objective to obtain images of 512 $\times$ 512 pixels (133.6 μm $\times$ 133.6 μm) at a scan speed of ~1 s/frame. A narrow beam (area 0.5 μm^2) from the Ti:sapphire laser was tuned to 760 nm for one iteration, resulting in deposition of 1–2 nJ on a single fiber. Sequential images were obtained for up to a total of ~30 min postablation.

Data analysis

Images obtained with the Zeiss LSM 510 software were imported into ImageJ (National Institutes of Health (NIH), Bethesda, MD) to determine

area changes before and after laser ablation. SF retraction dynamics were determined from the SF trajectory postablation from sequential images, and the data were fit to a Kelvin-Voigt model described by a viscoelastic time constant (τ) and a plateau retraction distance (L_o) as previously described:

$$L = L_o\left(1 - \exp\left(-t/\tau\right)\right) + D_a \quad (1)$$

Here L is the distance retracted, which is defined as half the distance between the two severed ends. D_a is the length of SF that is destroyed in the ablation event (like τ and L_o, this is a fitted parameter extracted from the experimental data).

We also employed spatiotemporal image correlation spectroscopy (STICS) (26) using software downloaded from the Wiseman group's Web site (http://wiseman-group.mcgill.ca/software.php) to quantify relocalization of actin fluorescence in response to pharmacological treatments. Briefly, STICS calculates the flow and velocity of fluorescent aggregates by tracking the displacement of the spatial autocorrelation function as a function of time—in our case, over a series of discrete time-lapse frames. In short, any directed motion will result in the displacement of the spatial autocorrelation function as a function of time. Division of the displacement per frame by the time per frame yields an average velocity expressed as displacement per time. We divided our confocal images into 32 pixel × 32 pixel grids for vector analysis and superimposed these vectors over the confocal images to produce a map that expresses the direction and magnitude of flow velocities throughout the cell.

RESULTS

Regional regulation of SF assembly by MLCK and ROCK

As described above, tensile prestress in SFs is derived from the contractile activity of NMMII, and previous studies in cultured fibroblasts have suggested that SFs located at the cellular periphery and center are predominantly activated by MLCK and ROCK, respectively. We previously showed that U87MG and U373MG human glioma cells form robust SF networks and display strongly mechanosensitive adhesion, migration, and proliferation (5). To confirm that this subcellular compartmentalization of NMMII-based SF regulation also holds in these cells, we cultured U87MG and U373 MG cells on collagen-coated glass, pharmacologically inhibited either ROCK or MLCK, and used immunofluorescence to examine the effect on the spatial distribution of SFs (Fig. 1 *A*, and Fig. S1 and Fig. S2 in the Supporting Material). Pharmacological inhibition of ROCK led to disassembly of central fibers and a dramatic conversion to a spindle-like morphology. In contrast, peripheral SFs largely remained intact. Conversely, MLCK inhibition led to dissipation of peripheral SFs and retention of fibers in the central region of the cell. This was frequently accompanied by the appearance of lamellipodial ruffles at the cell periphery. Of note, similar MLC-positive striations were observed in a given SF population either in the presence or absence of the other population, suggesting retention of contractile properties after drug treatment. A key limitation of immunofluorescence imaging is that it precludes longitudinal tracking of specific SFs. This is particularly problematic for interpreting MLCK inhibition studies, in which the resulting lamellipodial ruffles may superficially resemble peripheral SFs in a static image. To overcome this limitation, we fluorescently labeled the actin cytoskeleton by stably expressing mCherry-LifeAct in U373 MG and U87 MG cells, and obtained time-lapse images after drug treatment. Indeed, the central and peripheral SFs were selectively disrupted within tens of minutes after addition of the ROCK or MLCK inhibitors, respectively (Fig. 1 *B*, Movie S1, and Movie S2). To quantify the redistributions of actin subunits, we analyzed these time-lapse studies using STICS, which permits one to visualize flows of fluorescence intensity based on autocorrelation analysis (26). Vector maps obtained with STICS revealed a centrifugal flow of actin toward the periphery upon ROCK inhibitor-induced dissolution of central fibers and a centripetal flow toward the cell center upon MLCK inhibitor-induced dissolution of peripheral fibers (Fig. 1 *C*). Arrows in these images represent the magnitudes and directionalities of the autocorrelation of fluorescence intensity averaged over 80 min after drug treatment. Overall, these effects are consistent with previous results obtained in fibroblasts, implying that similar regional SF control mechanisms also operate in U373MG and U87MG glioma cells, i.e., ROCK preferentially regulates central SF assembly and contractility, and MLCK preferentially regulates peripheral SF assembly and contractility.

Selective disruption of central and peripheral SFs

Given that central and peripheral SFs appear to be regulated by different NMMII activators, we reasoned that these fibers' contractile properties and contributions to cell shape might differ as well. To test this hypothesis, we applied femtosecond laser nanosurgery, which we previously showed can selectively incise single SFs in living cells with submicron resolution and minimal collateral damage and without compromising cell viability (18,22,27), to photodisrupt and induce recoil of single central or peripheral SFs (Fig. 2, Fig. S3, and Fig. S4). Consistent with our previous studies, irradiation of each SF type led to immediate scission and continuous retraction of the severed ends on a timescale of 10–30 s without apparent damage to neighboring parallel fibers. Occasionally, fiber irradiation led to the formation of prominent blebs throughout the cell on the timescale of 5–10 min (Movie S3) followed by cell rounding or detachment, which we took as evidence that the plasma membrane had been compromised; such cases were excluded from further analysis.

Distinct viscoelastic recoil of central and peripheral SFs

The recoil dynamics of both central and peripheral SFs were well described by a Kelvin-Voigt model defined by a viscoelastic time constant, τ, and a plateau retraction

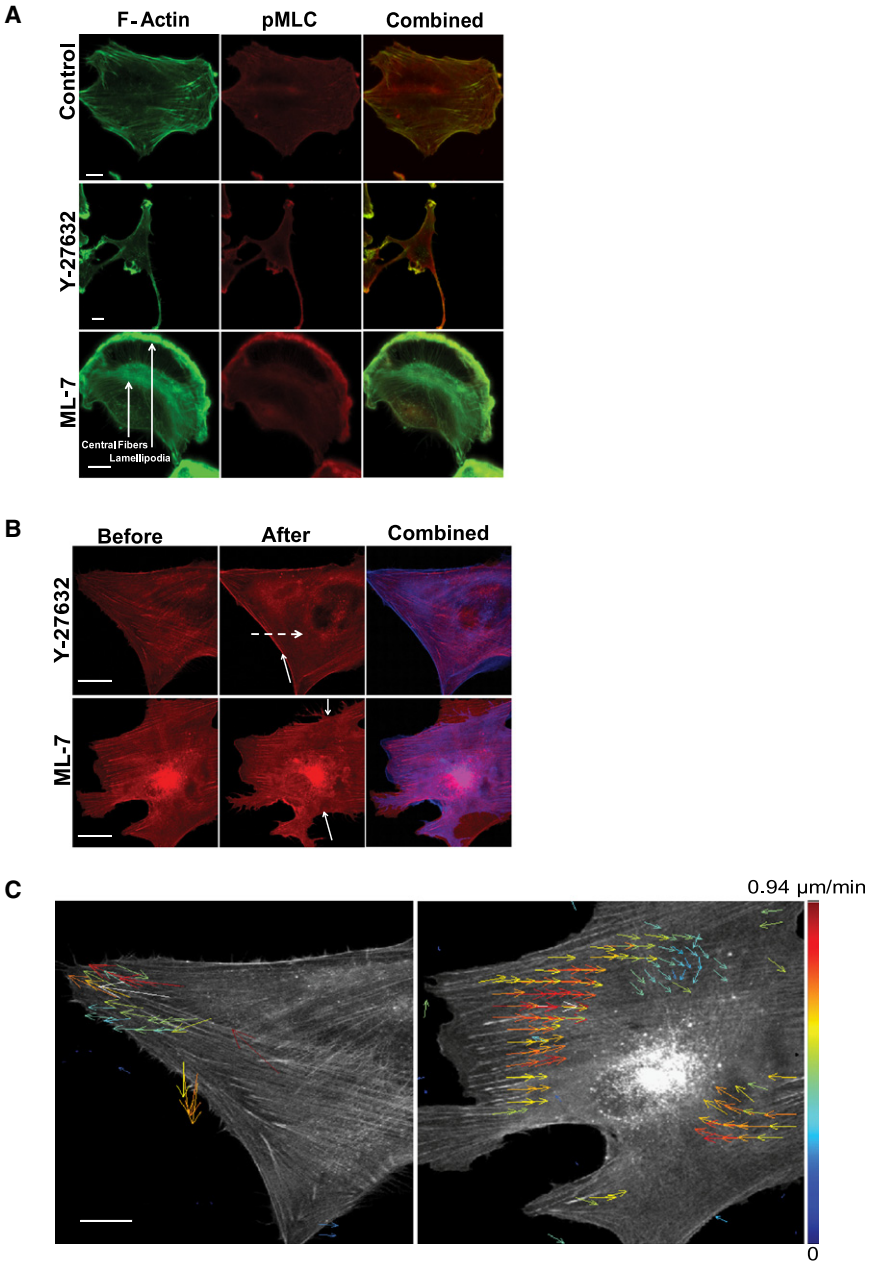

FIGURE 1 Regional control of SFs by ROCK and MLCK. (*A*) Immunofluorescence images of U373 MG cells showing F-actin (*green*, *left column*), pMLC (*red*, *middle column*), and regions of colocalization (*yellow*, *right column*). The top, middle, and bottom rows depict untreated control cells, cells treated with the ROCK inhibitor Y-27632 at 10 μM, and cells treated with the MLCK inhibitor ML-7 at 10 μM, respectively. The arrows in the bottom-left image denote the locations of an SF and lamellipodium, respectively. Bar = 10 μm. (*B*) Time-lapse fluorescence image of SF dissipation in response to ROCK and MLCK inhibition. The top left, middle, and right panels show a cell before Y-27632 treatment, after Y-27632 treatment for 80 min, and a before/after overlay, respectively. The solid arrow indicates reinforcement of peripheral fiber, and the dashed arrow shows the dissolution of central fiber. The bottom panels depict the same for the MLCK inhibitor ML-7. The bottom arrow indicates the loss of a peripheral fiber. Scale bar = 50 μm. (*C*) STICS velocity map of actin flow in response to pharmacological inhibition of ROCK and MLCK. Left and right panels show velocity maps for the average directed flow of actin toward the periphery of the cell after treatment with Y-27632 (*left*) and ML-7 (*right*), respectively, averaged over a total of 80 min for a total of 128 frames. Bar = 50 μm.

distance, L_o (18) (Fig. 3 depicts representative individual retraction curves; also see Movie S4 and Movie S5). Moreover, the shapes of the curves were different, with peripheral SFs typically retracting with larger time constants (i.e., lower effective elasticities) and larger plateau distances (higher apparent prestressed lengths) compared to central SFs—a finding that was consistent across different culture models (see Fig. 5 *C* for quantification and statistical analysis). These results demonstrate that femtosecond laser nanosurgery can selectively disrupt central and peripheral SFs, and that both fibers behave as viscoelastic cables, albeit with dramatically different viscoelastic properties.

Distinct contributions of central and peripheral SFs to cell adhesion and morphology

SFs stabilize cell shape by generating tensile forces that are transmitted through focal adhesions and opposed by the elasticity of the ECM. Thus, we asked how disruption of single central and peripheral fibers might alter cellular structure and adhesion (Fig. 4 and Fig. S5). Consistent with our earlier study, only slight cell-shape changes were observed upon irradiation of either type of SF on the timescale of retraction (i.e., 10–60 s). However, when we continued to observe cells over longer timescales of 2–20 min, we

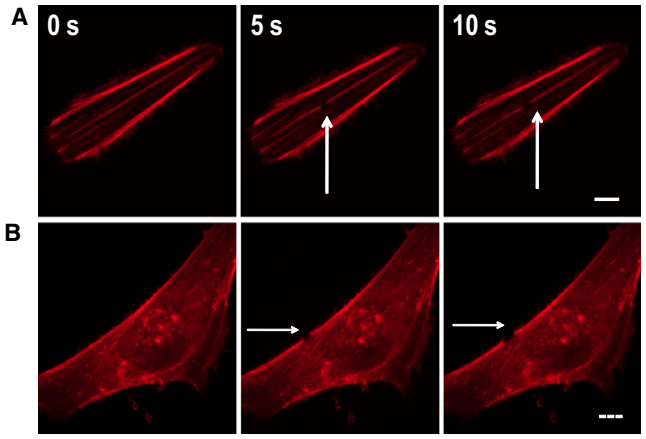

FIGURE 2 Selective photodisruption and viscoelastic recoil of central and peripheral SFs. (*A*) Photodisruption of a central fiber showing the kinetics of retraction after irradiation. Solid bar = 10 μm. (*B*) Photodisruption of a peripheral fiber. High-magnification images show retraction after ablation. Dashed bar = 20 μm. Arrows indicate the location of photodisruption. $N > 20$ SFs were ablated per condition.

noticed that photodisruption of peripheral fibers was often followed by disengagement of terminal adhesions and wholesale retraction of the entire cell (15–20% reduction in projected cell area; see Fig. 6 *B* for quantification and statistical analysis, and Fig. S6 for quantification of the dynamics of area change). In contrast, disruption of central SFs produced only minor (<5%) changes in projected cell area on this same timescale. Again, this result held for

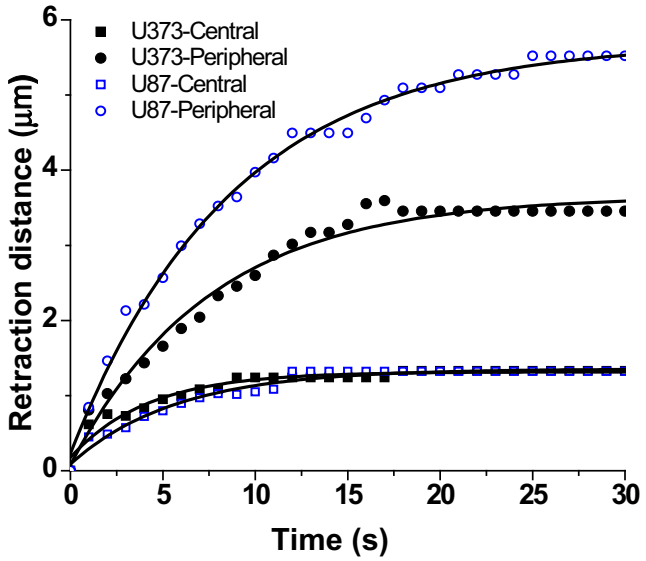

FIGURE 3 Representative recoil trajectories and fits for central and peripheral SFs. Retraction kinetics for a single central SF (*squares*) and peripheral SF (*circles*) irradiated in U373 MG cells (*solid symbols*) and U87 MG cells (*open symbols*). The solid lines are fits to a Kelvin-Voigt model for viscoelastic retraction. See Fig. 5 for means and statistical analysis of multiple SFs.

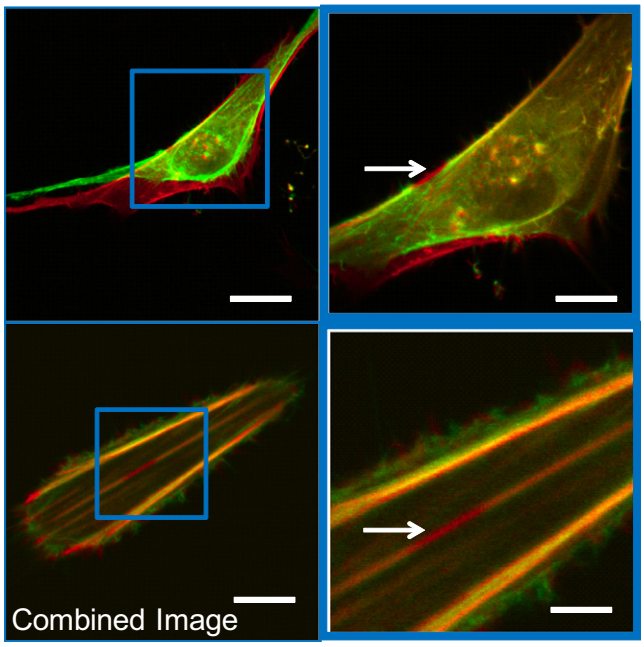

FIGURE 4 Representative images of area changes due to photodisruption of central and peripheral SFs. Negligible changes in cell area occur when a single central fiber is photodisrupted (*top*), whereas dramatic changes in cell area follow the ablation of a single peripheral fiber (*bottom*). Left: Low-magnification snapshots showing the outline of the entire cell. Right: High-magnification zooms of the boxed regions that more clearly show the severed SF. All images are overlays of mCherry-LifeAct fluorescence before ablation (*red*) and 30 min postablation (*green*). See Fig. 6 for means and statistical analysis of multiple cells. Scale bar for left and right panels = 10 μm and 20 μm, respectively.

both U87MG and U373MG human glioma cells, with only modest differences between cell lines.

One potential explanation for the above data is that peripheral fibers may be wider than central fibers and thus make stronger contributions toward maintaining cell shape independently of their subcellular location. To exclude this possibility, we measured the widths of each ablated SF by fitting the full width at half-maximum of a Gaussian profile of the image of the fiber. We failed to find significant mean differences in fiber widths across the two populations, at least at the resolution of confocal fluorescence imaging (0.7 $\pm$ 0.1 μm, 0.6 $\pm$ 0.1 μm for peripheral and central fibers, respectively). Additionally, to rule out the possibility that cells might be undergoing these shape changes because of laser-induced cell death, we continued to image cells for 30 min postablation. Even in cases where cells altered their projected cell area by 15–20%, we failed to observe overt signs of apoptosis, such as cell rounding, compaction, or blebbing. Such cells also successfully retained the vital dye Calcein AM while showing no signs of apoptosis as indicated by propidium iodide uptake (data not shown). In some cases, we even observed reformation of the severed peripheral fiber on the timescale of 30–60 min (Movie S6).

Spatio-regulated subcellular contractility

Given that SFs located in different regions of the cell are differentially regulated by myosin activators and exhibit different viscoelastic properties, we postulated that the two populations might play complementary mechanical roles, and that disruption of one population of SFs might alter the mechanics of the other population. To explore this possibility, we disrupted central and peripheral fibers by pharmacologically inhibiting ROCK and MLCK as before, and used femtosecond laser nanosurgery to measure the viscoelastic properties of the remaining populations. In most cases, fiber retraction continued to follow viscoelastic retraction kinetics (Fig. 5, *A* and *B*); however, the details of this retraction changed dramatically. First, disruption of central SFs by ROCK inhibition essentially abolished retraction of both the peripheral SFs and the few central fibers that remained, as evidenced by the retraction curves, which show a sudden jump to ~1 μm followed by a plateau. In sharp contrast, dissipation of peripheral SFs by MLCK inhibition slightly reduced the effective elasticity of central SFs (Fig. 5 *C*). This was accompanied by an increase in the plateau retraction distance for the central fibers (Fig. 5 *D*), consistent with the notion that the central SF assumes the mechanical role of peripheral SF when the latter population is removed. Morphometric analysis of area change for MLCK-inhibited cells revealed a significant long-term change in projected cell area when a single central fiber was disrupted, in strong contrast to what we observed in untreated cells (Fig. 4). A similar analysis of ROCK-inhibited cells showed minimal change in area in response to single SF ablation, regardless of its location in the cell (average changes are shown in Fig. 6). Together, these data suggest that there is transference of mechanical functions between regional populations of SFs, with pharmacological dissipation of MLCK-dependent peripheral SFs strongly altering the viscoelastic properties and cell-shape contributions of ROCK-dependent central SFs.

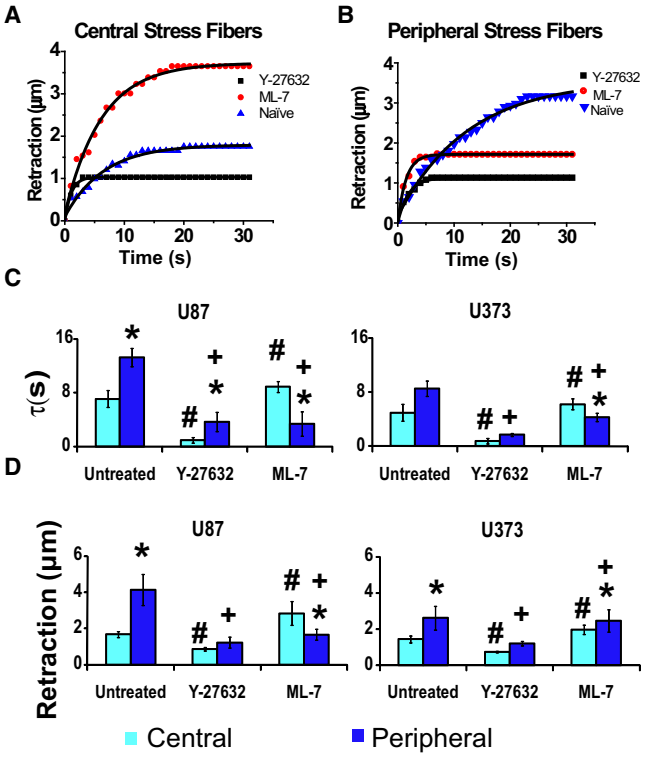

FIGURE 5 Effect of pharmacological inhibition of MLCK and ROCK on viscoelastic retraction. (*A* and *B*) Representative data and fits for central SFs (*A*) and peripheral SFs (*B*) when severed in untreated control cells (*triangles*), cells treated with ML-7 at 5 μM (*circles*), and cells treated with Y-27632 at 5 μM (*squares*) for U87MG cells. (*C* and *D*) Quantification of viscoelastic time constant (*C*) and plateau retraction distance (*D*) for central and peripheral SFs under drug conditions in *A* and *B* and for both U87MG and U373MG cells. In all cases, nanosurgery was conducted 3 h after administration of the drug. All comparisons are statistically significant ($p < 0.01$) as determined by a Student's *t*-test (unpaired, two-tailed, 95% confidence interval), where * denotes comparisons between central and peripheral fibers for each condition, and # and + denote comparisons between untreated and drug-treated for central (#) and peripheral (+) fibers. Error bars represent the mean ± SE, and $N > 20$ SFs per condition were ablated.

DISCUSSION

In this study, we used femtosecond laser nanosurgery to selectively measure the viscoelastic recoil behavior of two populations of actomyosin SFs in cultured glioma cells: ROCK-regulated central SFs that span the cellular interior, and MLCK-regulated peripheral SFs that define the cellular perimeter. By directly demonstrating that these two populations of SFs bear very distinct mechanical properties and cell-shape contributions, our study answers a question that was originally posed by Katoh and colleagues over a decade ago and has subsequently remained an open question in the field. Importantly, we arrived at this answer by conducting our experiments in the context of living cells with intact and functional cytoskeletal and adhesive machineries. These findings both complement and represent an important advance beyond studies that have relied solely on isolated SF preparations.

Perhaps our most significant findings are that 1), whereas peripheral SFs retract with lower effective elasticities than central SFs, they do so to much greater final retraction distances; and 2), disruption of peripheral SFs uniquely triggers profound cellular retraction on the timescale of minutes, suggesting that peripheral fibers play a particularly critical role in stabilizing cell-ECM adhesions and can compensate for central fibers once they are ablated. Both of these results are consistent with Katoh and colleagues' (28) earlier studies showing that stimulation of MLCK activity in isolated SF preparations yielded more extensive contractions than stimulation of ROCK activity, and that ML7-mediated disruption of peripheral SFs was accompanied by a loss of the cells' spread morphology (15). Intriguingly, our results also imply that in the absence of peripheral SFs (i.e., after MLCK inhibition), central fibers can mimic

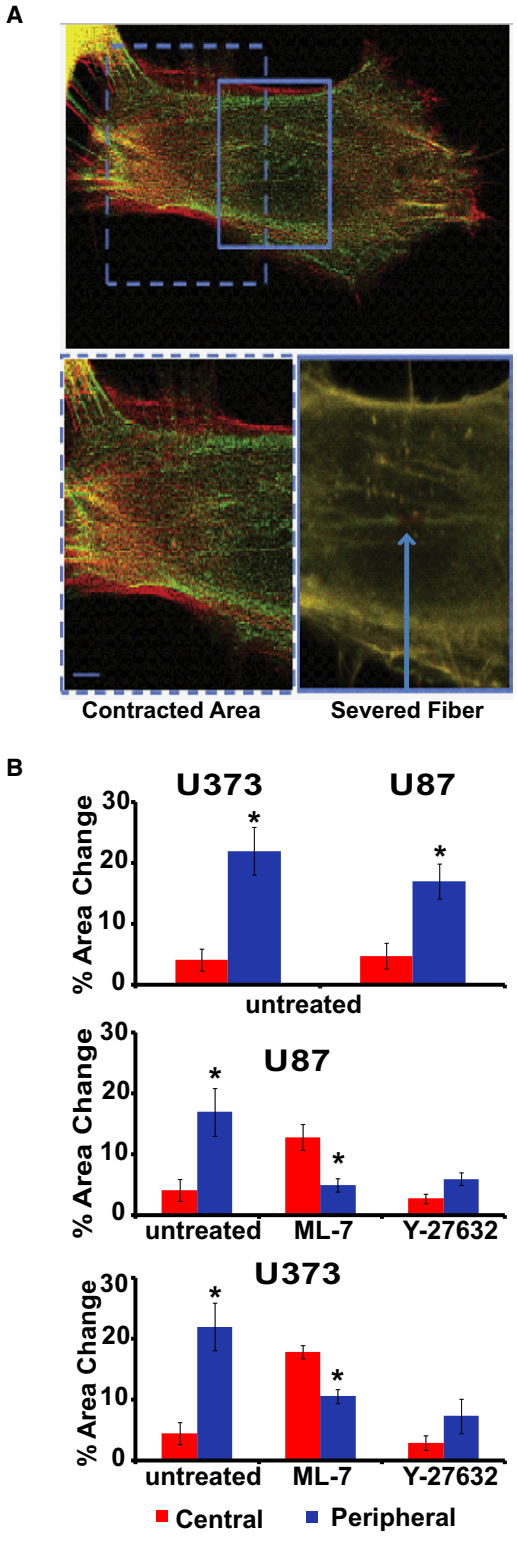

FIGURE 6 Effect of pharmacological inhibition of MLCK and ROCK on cell area over long timescales. (*A*) Effect of MLCK inhibition on central fibers. In cells treated with 5 μM of ML-7, photodisruption of a central fiber induces a dramatic change in area, whereas photoablation of a remaining peripheral fiber shows a negligible change in area. All images are overlays of mCherry-LifeAct fluorescence before ablation (*red*) and 30 min postablation (*green*). The bottom images are high-magnification zooms of the boxed regions in the top image. (*B*) Quantification of area changes as a function of location of the severed fiber. Top panel: Area changes for untreated control cells. Middle panel: Area changes in U87 cells treated with ML-7 and Y27632. Bottom panel: Area changes in U373 cells treated with ML-7 and Y27632, emphasizing the transference of tension in response to ablation of SF subpopulations. * Statistically significant area changes ($p < 0.01$) as determined by a Student's *t*-test (unpaired, two-tailed, 95% confidence interval). Error bars represent the mean ± SE for central versus peripheral for each condition. $N > 20$ SFs per condition were ablated.

both of these mechanical behaviors, in that they retract to greater plateau distances than in untreated cells, and their disruption produces cell-shape changes similar to those induced by disruption of peripheral SFs in untreated cells. This result in turn suggests that tensile loads previously borne by peripheral SFs may be transferred to central SFs when the former population is pharmacologically dissipated. Our STICS analysis demonstrates that pharmacological dissipation of a given SF population triggers a flow of actin subunits to the other population, which leads us to speculate that the mechanical mimicry may derive from the transfer of actin and potentially population-specific molecular components such as myosin and other actin-binding proteins. Interestingly, this effect is qualitatively much more prominent when the peripheral fibers are dissipated (compare the images in Fig. 1 *C*), consistent with the finding that although central fibers can mimic peripheral fiber properties, the reverse does not occur. The composition of this material flow remains an open question that investigators may be able to address in the future by directing STICS against a broader panel of SF molecular components. In any case, these studies would not have been possible without a technology capable of selectively disrupting single SFs in specific locations of the cell, which highlights the promise of laser nanosurgery-based approaches for investigating the bidirectional relationship between physical and biochemical control of cell shape and mechanics.

In addition to lending insight into myosin-based control of SF function in the cell, our studies further illustrate the potential of laser nanosurgery for mechanically mapping cytoskeletal mechanics in living cells. We and others (18,19,21,29,30) have previously demonstrated the ability of femtosecond laser nanosurgery to disrupt micronscale subcellular structures, including SFs, mitochondria, and microtubules, and our study shows for the first time, to our knowledge, that this technology can also be used to detect variations in the mechanical properties of cellular contractile elements on the microscale and correlate those results with differential modes of biochemical regulation. An important limitation of this approach as a mapping strategy is that compromising one SF will alter the loads borne by other SFs, meaning that one cannot independently probe the viscoelastic properties of multiple SFs in the same cell. In systems with significant cell-to-cell shape heterogeneity, it may be difficult to compile maps by combining results from multiple cells. One solution to this problem

may be to combine this technology with single-cell micropatterning, which yields relatively predictable SF architectures (31).

Our interpretation emphasizes the orthogonality of MLCK and ROCK in regulating contractile properties of specific SF populations. Importantly, however, we cannot completely rule out the possibility that there may be MLCK-dependent motors in the central SFs, and therefore MLCK inhibition may directly alter the behavior of central SFs. With that said, we note that our time-lapse imaging does not reveal appreciable morphological rearrangements in the central fiber population after ML7 treatment. Moreover, Totsukawa and colleagues (17) directly visualized MLCK in fibroblasts and found overwhelming localization to peripheral rather than central fibers. Future studies in which ROCK or MLCK can be inhibited in a spatially defined fashion in specific portions of the cell (e.g., by using photolabile probes or microfluidic drug delivery strategies) should definitively resolve this question.

The viscoelastic retraction we observed in this study confirms our earlier observations of SF retraction dynamics in capillary endothelial cells (18), but the cell-shape contributions are somewhat different. In our earlier study, we found that compromise of single SFs altered cell shape only when the cells were cultured on compliant (E ~ 4 kPa) ECMs. However, it is important to note that in the earlier study, cell-shape changes occurred concurrently with SF retraction (i.e., on the timescale of seconds), whereas in the study presented here, those changes occurred on the timescale of minutes. Thus, it is likely that the shape changes we observed here reflect force-dependent remodeling of focal adhesions rather than merely the passive cell elongation we observed previously. Moreover, it is remarkable that SF dynamics are relatively consistent across multiple cell types (our previous studies were conducted with endothelial cells, this study used glioma cells, and the studies of Katoh and colleagues were largely conducted with fibroblasts). This is reflected in our study by the observation that U-87 MG and U-373 MG glioma cells yield qualitatively and in some cases even quantitatively similar results for all measurements presented. This implies that the mechanisms of spatially dependent regulation of SF mechanics are highly conserved among adhesive cells, and provides reason for our optimism that this approach will prove useful for studying multicellular tissues and cell-ECM interactions.

Our observation that the severing of a single peripheral SF could radically alter cell shape can be placed in the context of other recent findings that actin-based cytoskeletal structures can communicate mechanical information rapidly and over tens of microns within the cell. For example, Wang and Suo (32) recently demonstrated that when ECM-coated magnetic beads are bound to integrins and twisted, displacement of mitochondria is observed as far as 30 μm away. More recently, Na et al. (33) showed that such mechanical inputs can trigger Src activation much more rapidly than those elicited by chemical stimulation of growth factor receptors. Pertinent to these findings, we observed a direct coupling between dissipation of tension in a single SF and disassembly of adhesions at the opposite end of the cell, several microns away from the site of incision (Fig. 4). This rapid change in morphology, which can begin to occur as quickly as 2 min postablation, suggests that these forces can be transmitted relatively quickly through the actomyosin network.

In summary, in this work we used femtosecond laser nanosurgery to investigate the viscoelastic retraction and cell-shape contributions of ROCK-regulated SFs located in the cell center and MLCK-regulated SFs located at the cell periphery. We have shown that these two populations exhibit significantly different viscoelastic retraction behaviors, and that disruption of peripheral SFs can trigger retraction of the entire cell on the timescale of minutes. Moreover, these two populations are mechanically interdependent, with pharmacological dissipation of one population strongly altering the mechanical properties of the other. In addition to addressing a longstanding question about the role of SFs in regulating cell shape, adhesion, and traction forces, our study illustrates the power of laser nanosurgery for spatially dissecting the contractile machinery of living cells at the microscale.

SUPPORTING MATERIAL

Six movies and six figures are available at http://www.biophysj.org/biophysj/supplemental/S0006-3495(10)01101-X.

We thank Dr. William Curtis Hines, Dr. Mandana Vesieh, and Doug Brownfield for their careful review of the manuscript and insightful comments. The STICS software was freely downloaded from the Web site of the Wiseman research group (McGill University; http://wiseman-group.mcgill.ca/software.php). ImageJ was freely downloaded from http://rsbweb.nih.gov/ij/download.html.

S.K. received grants from the National Science Foundation (CMMI 0727420) and the NIH Physical Science-Oncology Center (1U54CA143836), an Arnold and Mabel Beckman Young Investigator Award, and an NIH Director's New Innovator Award (1DP2OD004213), a part of the NIH Roadmap for Medical Research. K.T. received a postdoctoral fellowship from the U.S. Department of Defense Breast Cancer Research Program (W81XWH-09-1-0666). A.B. received a dissertation award from the California Breast Cancer Research Program (14GB-0007). The work from M.J.B.'s laboratory is supported by grants from the U.S. Department of Energy, Office of Biological and Environmental Research, a Distinguished Fellow Award to M.J.B., and Low Dose Radiation Program (contract No. DE-AC02-05CH1123); by the National Cancer Institute (awards R37CA064786, U54CA126552, R01CA057621, U54CA112970, U01CA143233, and NCI U54CA143836-Bay Area Physical Sciences–Oncology Center, University of California, Berkeley, CA); and by the U.S. Department of Defense (W81XWH0810736).

REFERENCES

1. Chen, C. S., M. Mrksich, …, D. E. Ingber. 1997. Geometric control of cell life and death. *Science.* 276:1425–1428.
2. Ewald, A. J., A. Brenot, …, Z. Werb. 2008. Collective epithelial migration and cell rearrangements drive mammary branching morphogenesis. *Dev. Cell.* 14:570–581.

3. Farge, E. 2003. Mechanical induction of twist in the *Drosophila* foregut/stomodeal primordium. *Curr. Biol.* 13:1365–1377.
4. Paszek, M. J., N. Zahir, …, V. M. Weaver. 2005. Tensional homeostasis and the malignant phenotype. *Cancer Cell.* 8:241–254.
5. Ulrich, T. A., E. M. de Juan Pardo, and S. Kumar. 2009. The mechanical rigidity of the extracellular matrix regulates the structure, motility, and proliferation of glioma cells. *Cancer Res.* 69:4167–4174.
6. Boudreau, N., C. J. Sympson, …, M. J. Bissell. 1995. Suppression of ICE and apoptosis in mammary epithelial cells by extracellular matrix. *Science.* 267:891–893.
7. Deguchi, S., T. Ohashi, and M. Sato. 2006. Tensile properties of single stress fibers isolated from cultured vascular smooth muscle cells. *J. Biomech.* 39:2603–2610.
8. Etienne-Manneville, S., and A. Hall. 2002. Rho GTPases in cell biology. *Nature.* 420:629–635.
9. Hotulainen, P., and P. Lappalainen. 2006. Stress fibers are generated by two distinct actin assembly mechanisms in motile cells. *J. Cell Biol.* 173:383–394.
10. Allen, W. E., G. E. Jones, …, A. J. Ridley. 1997. Rho, Rac and Cdc42 regulate actin organization and cell adhesion in macrophages. *J. Cell Sci.* 110:707–720.
11. Amano, M., K. Chihara, …, K. Kaibuchi. 1997. Formation of actin stress fibers and focal adhesions enhanced by Rho-kinase. *Science.* 275:1308–1311.
12. Guasch, R. M., P. Scambler, …, A. J. Ridley. 1998. RhoE regulates actin cytoskeleton organization and cell migration. *Mol. Cell. Biol.* 18:4761–4771.
13. Ridley, A. J., and A. Hall. 1992. The small GTP-binding protein rho regulates the assembly of focal adhesions and actin stress fibers in response to growth factors. *Cell.* 70:389–399.
14. Ridley, A. J., and A. Hall. 1994. Signal transduction pathways regulating Rho-mediated stress fibre formation: requirement for a tyrosine kinase. *EMBO J.* 13:2600–2610.
15. Katoh, K., Y. Kano, …, K. Fujiwara. 2001. Stress fiber organization regulated by MLCK and Rho-kinase in cultured human fibroblasts. *Am. J. Physiol. Cell Physiol.* 280:C1669–C1679.
16. Katoh, K., Y. Kano, and S. Ookawara. 2007. Rho-kinase dependent organization of stress fibers and focal adhesions in cultured fibroblasts. *Genes Cells.* 12:623–638.
17. Totsukawa, G., Y. Yamakita, …, F. Matsumura. 2000. Distinct roles of ROCK (Rho-kinase) and MLCK in spatial regulation of MLC phosphorylation for assembly of stress fibers and focal adhesions in 3T3 fibroblasts. *J. Cell Biol.* 150:797–806.
18. Kumar, S., I. Z. Maxwell, …, D. E. Ingber. 2006. Viscoelastic retraction of single living stress fibers and its impact on cell shape, cytoskeletal organization, and extracellular matrix mechanics. *Biophys. J.* 90:3762–3773.
19. Russell, R. J., S. L. Xia, …, T. P. Lele. 2009. Sarcomere mechanics in capillary endothelial cells. *Biophys. J.* 97:1578–1585.
20. Colombelli, J., A. Besser, …, E. H. Stelzer. 2009. Mechanosensing in actin stress fibers revealed by a close correlation between force and protein localization. *J. Cell Sci.* 122:1665–1679.
21. Colombelli, J., R. Pepperkok, …, E. G. Reynaud. 2006. Laser nanosurgery in cell biology. *Med. Sci. (Paris).* 22:651–658.
22. Lele, T. P., J. Pendse, …, D. E. Ingber. 2006. Mechanical forces alter zyxin unbinding kinetics within focal adhesions of living cells. *J. Cell. Physiol.* 207:187–194.
23. Rauzi, M., P. Verant, …, P. F. Lenne. 2008. Nature and anisotropy of cortical forces orienting Drosophila tissue morphogenesis. *Nat. Cell Biol.* 10:1401–1410.
24. Sen, S., M. Dong, and S. Kumar. 2009. Isoform-specific contributions of α-actinin to glioma cell mechanobiology. *PLoS ONE.* 4:e8427.
25. Riedl, J., A. H. Crevenna, …, R. Wedlich-Soldner. 2008. LifeAct: a versatile marker to visualize F-actin. *Nat. Methods.* 5:605–607.
26. Hebert, B., S. Costantino, and P. W. Wiseman. 2005. Spatiotemporal image correlation spectroscopy (STICS) theory, verification, and application to protein velocity mapping in living CHO cells. *Biophys. J.* 88:3601–3614.
27. Heisterkamp, A., I. Z. Maxwell, …, D. E. Ingber. 2005. Pulse energy dependence of subcellular dissection by femtosecond laser pulses. *Opt. Express.* 13:3690–3696.
28. Katoh, K., Y. Kano, …, K. Fujiwara. 2001. Rho-kinase—mediated contraction of isolated stress fibers. *J. Cell Biol.* 153:569–584.
29. Botvinick, E. L., V. Venugopalan, …, M. W. Berns. 2004. Controlled ablation of microtubules using a picosecond laser. *Biophys. J.* 87:4203–4212.
30. Wakida, N. M., C. S. Lee, …, M. W. Berns. 2007. Laser nanosurgery of single microtubules reveals location-dependent depolymerization rates. *J. Biomed. Opt.* 12:024022.
31. Parker, K. K., A. L. Brock, …, D. E. Ingber. 2002. Directional control of lamellipodia extension by constraining cell shape and orienting cell tractional forces. *FASEB J.* 16:1195–1204.
32. Wang, N., and Z. Suo. 2005. Long-distance propagation of forces in a cell. *Biochem. Biophys. Res. Commun.* 328:1133–1138.
33. Na, S., O. Collin, …, N. Wang. 2008. Rapid signal transduction in living cells is a unique feature of mechanotransduction. *Proc. Natl. Acad. Sci. USA.* 105:6626–6631.